DETECTING CHANGE IN URBAN AREAS AT CONTINENTAL SCALES WITH MODIS DATA

by

Carly M Mertes

A thesis submitted in partial fulfillment of the requirements for the degree of

Master of Science
(Cartography / Geographic Information Systems)

at the

UNIVERSITY OF WISCONSIN-MADISON
2014

Abstract. Urbanization is one of the most important components of global environmental change, yet most of what we know about urban areas is at the local scale. Remote sensing of urban expansion across large areas provides information on the spatial and temporal patterns of growth that are essential for understanding differences in socioeconomic and political factors that spur different forms of development, as well the social, environmental, and climatic impacts that result. However, mapping urban expansion globally is challenging: urban areas have a small footprint compared to other land cover types, their features are small, they are heterogeneous in both material composition and configuration, and the form and rates of new development are often highly variable across locations. Here we demonstrate a new methodology for monitoring urban land expansion at continental to global scales using Moderate Resolution Imaging Spectroradiometer (MODIS) data. The new method focuses on resolving the spectral and temporal ambiguities between urban/non-urban land and stable/changed areas by: (1) spatially constraining the study extent to known locations of urban land; (2) integrating multi-temporal data from multiple satellite data sources to classify ca 2010 urban extent; and (3) mapping newly built areas (2000-2010) within the 2010 urban land extent using a multi-temporal composite change detection approach based on MODIS 250 m annual maximum enhanced vegetation index (EVI). We test the method in 15 countries in East-Southeast Asia experiencing different rates and manifestations of urban expansion. A two-tiered accuracy assessment shows that the approach characterizes urban change across a variety of socicoeconomic/political and ecological/climatic conditions with good accuracy (70-91% overall accuracy by country, 69-89% by biome). The 250 m EVI data not only improve the classification results, but are capable of distinguishing between change and no-change areas in urban areas. Over 80% of

the error in the change detection is related to human decision making or error propagation, rather than algorithm error. As such, these methods hold great potential for routine monitoring of urban change, as well as provide a consistent and up-to-date dataset on urban extent and expansion for a rapidly evolving region.

1. INTRODUCTION

The demographic transformation toward an urban world has pushed urbanization – population growth as well as the expansion of built-up areas – to the forefront of environmental and development agendas. The consequences of urbanization are largely contingent on the size, location, and configuration of development (Weng, 2001; Zhou et al., 2004), with many environmental impacts exacerbated when new growth is expansive and/or fragmented in form (Alberti, 2005). A meta-analysis of urban expansion indicates that local- to regional-scale studies are geographically biased, leaving even many large cities unstudied (Seto et al., 2011). Detailed maps on regional- to global-scale changes in urban land do not exist; previous efforts have been sample-based (Angel et al., 2005; Schneider & Woodcock, 2008), focused on one country (Homer et al., 2004; Wang et al., 2012), or drawn conclusions from datasets with substantial temporal and spatial mismatch and variability in how cities are defined (Seto et al., 2010). Routine monitoring of urban expansion across large areas could therefore provide the spatial information on patterns of urban growth that are essential for understanding differences in socioeconomic and political factors that spur different forms of development, as well the social and environmental impacts that result (Deuskar et al., 2014).

Several ca 2000 global maps of urban areas have been produced in the past decade (Bhaduri et al., 2002; Schneider et al., 2003; CIESIN, 2004; Elvidge et al., 2007). Although these maps are static depictions of urban areas largely dependent on the input data sources (e.g., remote sensing, nighttime lights, census data), they have shown the potential for large-area maps of urban extent/expansion for a large number of applications, including: assessment of arable land (Tan et al., 2005; Avellan et al., 2012), water quality/availability (McDonald et al., 2011), natural resources (Lambin &,Meyfroidt, 2011), habitat loss

(Radeloff et al., 2005) and biodiversity (Guneralp et al., 2013); air pollution monitoring and associated impacts to human health (Grimm et al., 2008; Cassiani et al., 2013); and regional-global modeling of climate (Oleson et al., 2008), hydrological (McGrane et al., 2014), and biogeochemical cycles (Nordbo et al., 2012; Zhao et al., 2013). At the same time, these maps have proven vital for investigating socio-economic issues such as population distribution (Jones et al., 2013), spatial patterns of disease risk (Tatem et al., 2007; Wilhelmi et al., 2013), poverty (Elvidge et al., 2009), and economic growth (Chen & Nordhaus, 2011), and for planning and policy in developing-country cities that lack this information (Scott et al., 2013; Deuskar et al., 2014).

While remote sensing for large-area land cover change mapping has become common in many types of landscapes (Zhang et al., 2003; Linderman et al., 2005; Hansen et al., 2013), mapping urban expansion globally has remained incredibly difficult: urban areas are rare, their features are small, they are heterogeneous in both material composition and configuration, and the form, rates, and spectral-temporal signatures of new land development are highly variable across locations (Jensen, 1999; Makov et al., 2005; Potere et al., 2009; Schneider et al., 2009; Schneider, 2012). In addition, cost and data availability generally necessitate the use of coarse or moderate resolution data for continental scale mapping, thereby compounding the issue of land cover 'mixing' due to the large pixel size.

The primary objective of this work was to develop a methodology suitable for mapping urban land expansion at continental to global scales. Building on our past work using Moderate Resolution Imaging Spectroradiometer (MODIS) data to map global urban extent (Schneider et al., 2003; 2009; 2010), we developed a methodology to resolve the spectral and temporal ambiguities between urban/non-urban land and stable/changed areas

by: (1) spatially constraining the study extent to known locations of urban land; (2) integrating multi-temporal data from multiple satellite data sources to classify ca 2010 urban extent; and (3) mapping newly built areas (2000-2010) within the 2010 urban land extent using a multi-temporal composite change detection approach based on MODIS 250 m annual maximum enhanced vegetation index (EVI) observations. This method is built on one critical assumption: any conversion of land to urban uses is unidirectional and absolute, and thus, any urban expansion 2000-2010 will still be urban land in 2010.

We test and implement this methodology for 15 countries in East and Southeast Asia (Figure 1, hereafter East Asia). In doing so, we set a second objective to generate a new dataset depicting recent urban land expansion across the region (Schneider et al., in review). The rapid economic growth and high rates of urbanization characterizing many areas in the region have resulted in a high demand for timely land information for researchers, land use managers, governing institutions and the private sector. The East Asia region also provides a sound test case for method validation, as the predominance of cloud cover and complex urban landscapes that characterize the region require that the methods are robust to missing and noisy data in addition to addressing the challenges of urban change detection and large area mapping. In the following sections, we outline the background, describe the methods and results, and finally, conclude with a discussion of lessons learned from this research.

2. BACKGROUND

To map urban change across large areas, we draw on four areas in the remote sensing literature: (a) change detection methods for urban areas, (b) global monitoring of urban land, (c) global monitoring of change across large areas, and (d) recent change detection approaches that exploit multi-temporal observations.

Urban change detection. Measuring urban expansion via satellite imagery has been an increasingly common and effective method of extracting urban characteristics since the 1980s (Martin et al., 1989; Ridd et al., 1990; Herold et al., 2002; Yuan et al., 2005; Deng et al., 2009). Early approaches focused on simple band ratios, image thresholding, and image differencing to discern broad-scale changes at the urban–rural fringe (Jensen & Toll, 1982; Howarth & Boasson, 1983), while more recent developments try to accommodate the high variability within the urban class by exploiting spatial or polarimetric dimensions in satellite datasets. Spatial information has been incorporated through object-oriented approaches like segmentation (An et al., 2007; Bhaskaran et. al., 2011; Taubenböck et al., 2012), as well as by adding window-based texture features (Shaban & Dikshit, 2001) or spatial statistics (Ghimore et. al., 2010) into pixel-based change detection processing streams. Recent studies have also explored data fusion approaches to integrate multi-resolution optical data (Jin-Song et al., 2009), or radar and optical data during preprocessing (i.e. signal-based, fusing raw data) (Amarsaikhan 2012) or classification (e.g. pixel-based, combining inputs within one algorithm) (Corbane et al., 2008; Griffiths et al., 2010; Zhu et al., 2012). With the proliferation of very high resolution (VHR) sensor systems, multisource fusion techniques have demonstrated their potential to increase map accuracy in urban areas, but are limited for

monitoring applications because of the infrequent revisit time and high data and processing costs. For similar reasons, these methods have only been applied at the scale of individual cities or neighborhoods (Pesaresi, 2000; Pacifici et al., 2009; Bhaskaran et al., 2011), where obtaining full coverage with high/very high resolution (VHR) optical data or radar images is feasible.

Global mapping of urban areas. Several studies have used self-consistent maps of individually classified cities for global-scale analysis of urban trends and typologies (Angel et al., 2005; Kasimu, 2005; Schneider & Woodcock, 2008; Wentz et al., 2009), although inconsistent methodologies and definitions of 'urban land' can impede cross-city analysis. During the last two decades, eight different teams have developed global maps that depict the spatial extent of urbanization ca 2000 (Gamba & Herold, 2009), while others have proposed methods that could be applied in the future (Zhang & Seto, 2011; Taubenböck et al., 2012). Unfortunately, the existing maps exhibit a great deal of variability in how urban areas are characterized, evident from the areal estimates of urban land given by these maps (from 300,000 to 3 mil km^2, Schneider et al., 2010). The definitional problems are twofold. First, any number of operational definitions of 'urban' are employed, ranging from functional definitions related to human land use (Balk et al., 2004; Zhang & Seto, 2011), administrative boundaries (Deichmann et al., 2001), or population size and density (Bhaduri, 2007), to physical ones based on land cover (Schneider et al., 2003; Elvidge et al., 2007) or anthropogenic light (NGDC, 2007). The second is whether the adopted definition is congruent with how the maps are produced, such that the input datasets, classification method, and thematic classes align with how urban areas are defined. Nearly all recent

efforts exploit optical data or nighttime lights data, and all utilize either semi-automated classification algorithms (Schneider et al., 2003; Bartholome & Belward, 2005; ESA, 2008) or data fusion methods that draw on a combination of satellite imagery, census data, and GIS datasets (Bhaduri et al., 2002; CIESIN, 2004; Goldewijk, 2005; Elvidge et al., 2007).

Most critically, few of the global urban mapping efforts – including new work by the European Space Agency and Google Earth Engine to map ca 2010 urban land – depict *changes* in urban land over time. The exception is the GeoCover Land Cover product for 1990-2000 (MDA Federal, 2004). GeoCover maps have limited coverage in the tropics, Europe and Central Asia, remain prohibitively expensive, and are becoming outdated for areas witnessing rapid changes since 2000 (Potere et al., 2009). More recent efforts using nighttime lights to monitor urbanization have been effective, but may have limitations for mapping urban land expansion explicitly as these data have found to be a function of demographic, socioeconomic, and land surface variables (Zhang & Seto, 2011; Ma et al., 2012).

Change detection over large areas. New access to Landsat and SPOT data has generated a boom in their use for large area applications (Wulder et al., 2012), yet several barriers to their widespread adoption are yet to be resolved. Data availability is still hampered by cloud cover (35% on average, Ju & Roy, 2008), gaps from the scan line corrector failure of Landsat 7 (22% per scene on average, Storey et al., 2005), and data discontinuities in the archives. In addition, processing these scenes for large areas remains time- and labor-intensive due to the small scene footprint (e.g., East Asia covers more than 1500 Landsat footprints). Meanwhile, the advantage of moderate/coarse resolution data for these applications is clear:

comprehensive areal coverage, large image scenes, routine monitoring, archival depth, and perhaps most importantly, frequent data acquisition (looks every 1-2 days). Moreover, many of the methods developed for these coarser resolution data will become viable for the analysis of Landsat data as technical solutions to address data quality and availability are developed.

Multi-temporal data to monitor change. The legacy of using moderate/coarse resolution data for land cover characterization (Lambin & Strahler, 1994; Borak et al., 2000) has resulted in the development of a rich array of methods to exploit temporal information in satellite data. Many methods that take advantage of multi-season and multi-year observations employ time-series spectral profiles, as the large number of data points provides better discrimination of signal from noise, and makes it possible to link vegetation phenology to the spectral trajectory (Kennedy et al., 2014). Curve-fitting (Zhang et al., 2003; Kennedy et al., 2007), harmonics analysis (Cihar et al., 2001; Jakubauskas et al., 2001; Bradley et al., 2007; Geerken, 2009), and wavelet transformation (Sakamoto et al., 2005; Martinez et al., 2009) have all been used to monitor vegetation dynamics and extract phenological markers (e.g. date of greenup, senescence) in forested or agricultural landscapes.

Other techniques take advantage of temporal compositing, which can significantly reduce data volumes while retaining the temporal variability related to land cover or phenological states (Borak et al., 2000; Clark 2012). While any metric may be used to summarize the time series, maximum value compositing of vegetation indices (VI) are most common, because it provides an informative measure of vegetation content while also reducing negatively-biased noise arising from cloud contamination (Fisher, 2006). To

monitor change, the maximum VI data are then often analyzed in a time series themselves (Rahman et al., 2013; Setiwan et al., 2014), or used as classification features in dense time series of spectral data (Alcantara et al., 2012; Clark et al., 2012. Recently, the 'dense time stacks' change detection method has been applied in urban areas where the added seasonal information helped to overcome spectral confusion between fallow cropland and new urban development (Schneider, 2012, Kontgis, in review).

3. DEFINITIONS

3.1 Defining urban areas and urban expansion

An important first step in the methodology is establishing a clear conceptual framework for defining and delineating the urban environment. Representations of urban areas derived from satellite data are most congruent with definitions based on the surface properties that they measure (Potere & Schneider, 2007). Therefore, we define urban areas as locations "dominated by the built environment", where dominated implies >50% coverage of a pixel (Schneider et al., 2009). Spaces that perform an urban function but are not made up of constructed surfaces, such as parks or golf courses, are not considered urban land. We also define a minimum mapping unit (MMU) of 0.56 km^2 (3x3 250 m pixels) as the smallest contiguous area of built-up land reliably represented using 250-500 m MODIS inputs.

The approach to monitor urban change is based on the premise that any conversion of land to urban cover 2000-2010 will appear as urban land in 2010. The assumption that urban land development is irreversible is commonly adopted for land change studies (Carrion-Flores & Irwin, 2004; Seto et al., 2011; Schneider, 2012; Taubenböck et al., 2012) and in practice holds true especially at the temporal scale of interest (e.g. decade). Housing

demolition does occur within the study region, but the result is land modification or redevelopment rather than land conversion. In this research, only conversion of non-urban to urban land is considered 'urban expansion,' and all areas converted to built-up surfaces are labeled urban expansion regardless of location near the city, or in peri-urban or rural areas.

3.2 Delineating the study area extent

We constrained the East/Southeast Asia study region to known locations of urban land. To do this, we synthesized all contemporary city point data available (gazetteers, city lists, etc., Table 1) with the 2001 MODIS map of urban extent (Schneider et al., 2009; 2010). Circa 2010 data were used in all cases possible to ensure all cities >100,000 – including those that grew from small villages to cities >100,000, 2000-2010 – were included in the study extent. In cases where city points did not align with 2001 urban areas, city point locations were manually checked in Google Earth and adjusted as necessary. Patches of urban land present in the MODIS map but lacking city points were similarly cross-checked and included in the dataset. Urban patches were categorized into small, medium, and large classes based on their areal extent and population, and then buffered by 5, 25, and 100 km, respectively, to create the final study extent. The final study extent represents 30% of the total land area in the region.

Previous work has demonstrated the value of biomes for stratifying data for continental-scale land cover change (Clark et al., 2012) and urban applications (Schneider et al., 2009). Climate, vegetation, and ecosystem characteristics all exert controls on land cover and the structure of human settlements, making biome designations particularly useful for data processing. Using Olson's biome classification (Olson et al., 2001), the study region

was delineated into nine biomes covering temperate, tropical and arid regions (Figure 1b). These designations were used for classification, change detection, and accuracy assessment.

4. DATA AND METHODS FOR MONITORING URBAN EXPANSION

4.1 Overview

After defining the study extent (Section 3.2), we characterize urban expansion 2000-2010 by: (1) classifying ca 2010 urban land, and (2) locating areas of change within the ca 2010 urban extent.

4.2 Remote sensing data

We exploit the spectral and temporal information in two separate sources of MODIS data: (1) MODIS 500 m multispectral data, and (2) MODIS 250 m enhanced vegetation index (EVI) data (Table 2). Specifically, we use MODIS 500 m Nadir BRDF-Adjusted Reflectance (NBAR) surface reflectance data (Schaaf et al., 2002) for the seven "land" bands (visible to mid-infrared) for 37 tiles in Asia. NBAR data are normalized to a nadir-viewing angle to reduce noise resulting from varying illumination and viewing geometries (Schaaf et al., 2002).

In the NBAR data, missing data frequently occur within/near cities since bright urban surfaces are often mistakenly removed during cloud screening (Leinenkugel et al., 2013). This problem is clear in Figure 2, where city extents exhibit a high percentage of missing data compared to surrounding areas. To minimize the effect of these data gaps, we developed an optimization algorithm that assessed missing data on a tile-by-tile basis for a sample of cities within each MODIS tile. Based on these results, a contiguous cloud-free

season was selected for each tile (between 11 and 21 8-day observations, Figure 2e). The 8-day observations were then aggregated to monthly composites to reduce the temporal correlation and the frequency of missing values from cloud cover. Monthly and yearly minima, maxima, means, and variances for each band and EVI were also estimated from the cloud-free season for each tile.

At 250 m resolution, we rely solely on EVI data, since vegetation removal has been shown to be an important indicator of urban land conversion (Stefanov et al., 2001; Schneider, 2012). Because raw MODIS 250 m data are noisy and have a large number of missing observations, we temporally smoothed the data using a modified asymmetric Gaussian filter within an augmented version of TIMESAT (Jonsson & Elklunh, 2002), and then fit a curve to the data that approximates the phenological pattern to fill data gaps (Gao et al., 2008; Tan et al., 2011). The result is a high-quality dataset shown to be suitable for both classification and direct assessment of EVI values (Tan et al., 2011). We selected the MODIS EVI data for the growing season in each tile (23 observations), and then computed the maximum EVI from these values for each year, 2001-2010.

4.3 Classification of 2010 urban extent

To classify 2010 urban extent, we rely on an ensemble method which uses a supervised decision tree as the base algorithm (C4.5, Quinlan, 1993). Decision trees are widely utilized in large area mapping of land cover (Friedl et al., 2002; Hansen et al., 2005) and urban areas (Schneider, 2009) where complex spectral datasets require robust algorithms. Decision trees are constructed through the recursive partitioning of training data according to a statistical test applied to the training features (here, an attribute value test of a spectral

feature which maximizes information gain at each split). After they are built, unlabeled pixels are sorted down the tree according to the decision rules and eventually terminate in a class assignment. Ten trees are estimated using boosting, a technique that improves class discrimination by iteratively training classifiers based on different weightings of the training data. Because a class label is assigned with each iteration of the boosting algorithm, together the ensemble of trees provides an estimate of conditional probabilities for each class at every pixel (McIver & Friedl, 2001). Although the optimization approach (Section 4.2) helped isolate the least cloudy season for each tile, we used three years of MODIS 500 m data (2009-2011) for the selected season to ensure at least one quality observation for each pixel.

The training data were built upon the System for Terrestrial Ecosystem Parameterization (STEP) database, a set of >2000 exemplars collected from Google Earth and Landsat data for 17 classes (Friedl et al., 2002; 2010). The database was augmented with sites drawn from a stratified random sample of 250 locations within the East-Southeast Asia region (Figure 3a, b). All sites were collected as 0.5-2.0 km^2 polygons of uniform land cover interpreted using VHR Google Earth imagery.

The results of the MODIS 500 m classification were promising (Figure 4a), but showed confusion between urban classes and mixed vegetation classes in areas outside cities. To resolve this issue, we employed a data fusion methodology to integrate 250 m MODIS EVI data with the class probabilities from the boosted decision trees (Figure 4). As demonstrated by past work (Schneider et al., 2010), urban areas may exhibit similar seasonal fluctuations in EVI as the surrounding vegetated classes, but achieve a distinct peak greenness. In tropical and temperate regions, EVI reaches a higher maximum in vegetated areas outside the city, while in arid/semi-arid regions, EVI is often higher within cities due to

vegetation planted near buildings and roads. We exploit these differences in growing season maximum in the 250 m EVI data to estimate *a priori* probabilities for urban land, which we use to adjust the conditional class probabilities from the 500 m data using Bayes' Rule.

To compute the prior probabilities, we defined a logistic regression model using the growing season maxima for the smoothed, gap-filled MODIS EVI data. The model is mathematically defined using a binomial distribution and the expression

$$P(U_{LR}) = \frac{e^{V_i}}{1 + e^{V_i}} \quad [1]$$

where $P(U_{LR})$ is the probability that a pixel is urban, and V_i is provided by a multiple linear regression model. Several trials were conducted to model the relationship between EVI and urban areas using different predictor variables (Table 3, models 1-5). Based on the predictive power of the model, given by the area under the receiver operating characteristic (ROC) curve, and the hypothesis test of each variable coefficient (Table 3), the results show that model 3 outperformed the others. Thus, we model V_i as:

$$V_i = \beta_0 + \beta_1 EVI2009_i + \beta_2 EVI2010_i \quad [2]$$

where $EVI2009_i$ and $EVI2010_i$ are the maximum EVI observations for 2009 and 2010 for the *i*th pixel, β_1 and β_2 are their coefficients, and β_0 is the intercept. Because of the increased spatial resolution of the imagery, we also found that a model trained with pixels selected from visual interpretation of the 250 m MODIS data outperformed the model trained with the

STEP exemplars selected in Google Earth (Table 3, models 6-7).

We constructed separate logistic regression models for temperate, tropical and arid regions (Figure 1b). Training data were collected for urban and non-urban sites for each model (Figure 3c) so greater local representation within each region could be achieved. The regression coefficients were estimated within Matlab (2011a, The MathWorks, Inc., Natick, MA, US) for each model using an iterative maximum likelihood estimation method for 80% of the training data. The remaining 20% of data were used to assess model performance (Table 4). The Wald test results confirmed that the coefficients for each model were significant at $p < 0.05$ and therefore contributed to the regression. The ROC areas were 92, 84, and 76% for temperate, tropical, and arid biomes, respectively, indicating that these models are suitable for predicting the presence of urban areas.

In the last step of the ca 2010 urban classification, we adjusted the conditional probabilities from the decision trees $P(U_{DT})$ by the *a priori* probabilities from the 250 m MODIS data, $P(U_{LR})$. Following Bayes' Rule, we estimate the posterior probabilities $P(Urban)$ as:

$$P(Urban) = \frac{P(U_{DT}) \cdot P(U_{LR})}{\sum_i P(U_{DT}) \cdot P(U_{LR}) + ((1 - P(U_{DT})) \cdot (1 - P(U_{LR})))} \quad [3]$$

We compare the posterior probabilities to Google Earth VHR imagery to select an appropriate threshold for defining the urban class on a tile-by-tile basis. These thresholds are selected at natural breaks in the data and vary by biome and by country, based on the local characteristics and data quality in each area. In temperate biomes, for example, urban areas

are spectrally distinct from surrounding vegetation types, there is distinct seasonality within the time series data, and there are sufficient high-quality training data and cloud-free observations. As a result, thresholds of >90% are used to define urban from non-urban areas in the posterior probabilities. In arid regions, however, the difficulty in characterizing urban land as distinct from surrounding cover types requires low thresholds (on average, 25%), with variability based on location. Finally, the lack of cloud-free imagery (and the classification difficulty that results) leads to the use of similarly low thresholds (on average, 41%) to create the final maps for tropical countries. Although the choice of threshold is subjective, the ability to vary these values relative to Google Earth observations is beneficial, since it allows us the opportunity to move away from 'one size fits all' classification methods.

Post-processing refinements were made to finalize the urban extent map. Spurious pixels were removed using a sieve filter, water bodies were masked using the MODIS 250 m land-water layer (Carroll et al., 2009), and problem areas were manually edited.

4.4 Mapping change areas (2000-2010)

Capitalizing on our assumption that urban land does not become ‘undeveloped’, the 2010 urban extent map was used to spatially constrain the change detection process. The change detection method used ten years of growing season maximum EVI data (2001-2010) as input to a boosted decision tree algorithm (C4.5) to classify the circa 2010 urban extent as: (1) built-up in 2000; or (2) urbanized during the 2000-2010 period. The localized training data collected for the logistic regressions (Figure 3c) were revisited, and all urban sites were labeled as existent urban land, or newly developed urban land, 2000-2010 (Figure 3d).

This approach relies on the observed relationship between EVI and urban areas previously established: any conversion from a non-urban land cover (agriculture, grassland, forest, etc.) to developed land is detectable through changes in vegetation content. As the magnitude and direction of change in vegetation signal may vary from region to region and between different initial land cover types (e.g. conversions from tropical forest to densely built-up areas will result in large drop in EVI, whereas a conversion from bare ground may actually result in an increase in EVI from tree and grass planting alongside roads and buildings), it was necessary to construct decision trees and choose breakpoints to threshold the decision tree output probabilities by subregion (temperate, tropical, arid) in a similar procedure used for the 2010 urban extent map (Figure 5).

5. RESULTS

5.1 Regional and local views

We present the change detection results in Figure 6 for a subset of metropolitan areas. Visually, these views are in accordance with ground-based evidence and spatial datasets produced at different time points and/or scales. They also indicate that the methods capture new urban development that is contiguous with the urban core across a range of city sizes, as well as patchy growth in peri-urban areas far from the city edge. The lack of available data on urban expansion at comparable scales limits our ability to cross-examine the map trends, but also underscores an important result: up-to-date, consistent, and spatially-explicit information on the extent and growth of cities is now available for the rapidly evolving regions of East and Southeast Asia.

5.2 Tier one accuracy assessment

We assess map accuracy using a two-tiered approach. First, we assess the quality of the 2010 urban classification results, followed by an evaluation of the change detection methodology and urban expansion map accuracy (Section 5.3). The tier one test sites were generated using Geodesic Discrete Global Grids (DGGs) (Sahr et al., 2003), a class of equal-area, uniformly distributed hexagonal partitions of the Earth's surface. To define the sites, we used a DGG with a facet size of 0.132 km^2 and a stratified random sample design drawn from within the study extent. While the final maps were produced at 250 m, this site-based analysis was designed to provide a sampling unit consistent in size with the training data and the 500 m grid of the coarsest resolution MODIS data. The sites were assessed in Google Earth using high resolution data (≤4 meters) in a double-blind assessment procedure by a team of photo-interpretation analysts. A final review of all sites was conducted for quality control and to assign labels in cases where analysts disagreed.

The overall accuracy of the 2010 map of urban extent (tier one) is 84% (kappa = 0.62), and is fairly consistent across countries (ranging from 79-93%, Figure 7) and biomes (83-100%, Figure 8). Producer's accuracy for the urban class is similarly high for the region (85%), indicating that urban areas are well captured, with few errors of omission (Tables 5, 6). At 64%, the user's accuracy for the region is reasonable but suggests that map errors are predominantly the result of commission errors, where non-urban areas area mislabeled as urban land. As a result, the total urban land area may be overestimated in some locations, particularly Thailand, Malaysia, and Laos, where user's accuracies are <61%.

5.3 Tier two accuracy assessment

The second tier assessment is designed to quantify the accuracy and efficacy of the change detection methodology, as well as evaluate the accuracy of the urban expansion maps. First, samples are selected in proportion to each country's share of urban land in the region (note that for countries with <1% of urban land, we use a minimum of 20 sites). Second, we sample across biomes, selecting sites in proportion to the distribution of urban land across nine biomes (Olson et al., 2001). Once the sample distribution was established (Table 7), we selected sites at random from within a tightly buffered region of the city points using the 250 m MODIS raster grid to ensure that the sample included urban expansion sites. Following the same procedure as in tier one, each site was assessed in Google Earth and assigned one of three labels: urban land, urban expansion, or non-urban land.

The overall accuracy for the urban expansion maps is 75% (kappa = 0.36), slightly lower than the overall ca 2010 accuracy. More developed countries (e.g. Japan, Taiwan, South Korea, etc) generally have higher accuracies (>80%) than other locations (Table 8) likely because of the low growth rates in these highly urbanized countries. Overall accuracy also tends to be higher in temperate and forest biomes than arid/semi-arid biomes (Table 9), as do the producer's accuracies (9 to 25% above average, 11 to 21% below average, respectively). This result is related to the spectral and temporal signatures of the EVI data used in change detection. In arid regions, EVI signatures before and after change are quite similar. Land outside the city that is spectrally bright and sparsely vegetated is converted to new urban land, which then also appears spectrally bright with minimal vegetation.

5.4 Redefining urban areas: applying a minimum mapping unit

While the objective of these mapping efforts was to capture all cities >100,000 persons, small cities and villages were also mapped in many areas where the size/composition of the settlements made them spectrally and temporally distinct (e.g., outside Beijing, Figure 6b). Small patches of urban land around cities were also mapped and remain in the dataset even after spatial filtering. In general, these areas – which range from one to nine pixels (0.06-0.56 km^2)– are mapped less confidently because data resolution and point spread function effects introduce considerable uncertainty at the scale of individual pixels. In this section, we examine the degree to which these small areas may contribute to the low accuracies described above. We first apply a minimum mapping unit (MMU) of 0.56 km^2 (nine 250 m pixels), remove urban patches below this value, and then re-estimate the tier one and tier two accuracy measures (Table 10). We subset the test sites to include only those where the class label remains unchanged between the original and the filtered maps.

The accuracies of both the ca 2010 urban extent and 2000-2010 expansion maps are modestly improved after the MMU is applied (1-2%), with only a small portion of the original test sample dropping (4-6%). This occurs because the tier one and tier two sampling techniques stratified the region based on city point locations; urban sites were mainly confined to cities >100,000 and rarely fell on smaller settlements. This limits our ability to report on how accurately the map represents these small settlements. The results confirm that the accuracy measures are not significantly affected by the inclusion of these patches and are representative of urban areas as defined in Section 3.1.

5.5 Sources of uncertainty and error in the maps

As expected, the tier two accuracy measures are lower than those for tier one, a result that is to be expected: the errors of the 2010 urban classification propagate through to the change detection maps, thus lowering the overall achievable accuracy from the start. To evaluate the methodology and the structure of possible map errors in a more targeted manner, we assessed the source of uncertainty for each misclassified site in the tier two results (n = 513). Each site was reevaluated in Google Earth to determine the likely source of error, and labeled accordingly (Table 11, Figure 9).

The distribution of errors clearly shows the sensitivity of the tier two assessment to the classification results: more than one third of errors are actually due to classification errors from the initial map of ca 2010 urban land (issue 1, Table 11). While obtaining a perfect classification of 2010 urban land is unrealistic, we can hypothesize that an error-free map of urban land might improve the change detection results. After removing sites mislabeled as non-urban land from the tier two sample, accuracies increase 5-15% depending on location, indicating that the change detection method is likely more effective than the overall accuracy results indicate (Figure 8).

Twenty-four percent of errors can be traced to the density threshold used to define urban land (issue 2, Table 11). In these cases, the site had some development in 2000 but was not sufficiently built-up to meet the definition of urban land (i.e. >50% built up). Like the first issue, this case traces back to the ca 2010 classification but is not a complete categorical error in labeling. Compounding the problem however is the fact that many of these same locations witnessed an increase in buildings or impervious cover over the 2000-

2010 decade (Figure 9b). The change detection algorithm does not recognize these areas as change, however, and the early 2000 time point is mislabeled as urban land.

Another issue related to the density threshold is that linked to redevelopment and infill (issue 3, Table 11). As some large cities expand, they consume small villages and built-up areas by clearing old buildings and replacing them with new, spectrally-bright development (Figure 9d). Likewise, in urbanized areas that are undergoing densification, the spectral response may increase dramatically with new construction. Because our definition of urban land included any built-up areas or settlements, these sites are technically 'urban' in 2000, and remain urban land in 2010. The spectral difference is often large, however, and the change detection approach characterizes these areas as urban expansion accordingly.

An additional 19% of the tier two errors are simply related to change detection errors where urban land is mislabeled urban expansion or vice versa, without an obvious indication as to the source of spectral or temporal confusion (issue 4, Figure 9d). Within this class of errors, the confusion between urban land and urban expansion occurs at a similar frequency, suggesting that there is no bias toward either over- or under-estimating change in the method itself.

6. DISCUSSION AND CONCLUSIONS

We present a new methodology that leverages information on the location and nature of urban areas and growth using multiple sources of moderate resolution remotely sensed data. In doing so, we address an important challenge that has limited large-area mapping of urban expansion: urban features are small and there is high variability in the spectral responses of urban areas. We tested the approach for a large and diverse region where urban

expansion is often uncoordinated and patchy, and consequently, where urban maps are most challenging to produce, yet most needed. The results reveal several insights for monitoring urban change that are relevant to future studies:

Satellite data fusion helps yield higher map accuracy in complex urban landscapes. While the amounts and quality of remote sensing data are unprecedented, there is still no one 'perfect' data source for the difficult task of mapping urban expansion. We will continue to face limitations in areal coverage and spatial detail, as well as missing data due to cloud cover. Missing or noisy observations have been shown to significantly impact final map accuracy even when advanced data mining algorithms are employed (Schneider, 2012). Many multisource data fusion approaches have been developed for remote sensing, whether to take advantage of multiple data types (e.g. multispectral, SAR, GIS, etc.), multiple spatial resolutions, or multiple remote sensing domains (e.g. spatial, temporal, etc). For example, pan-sharpening – a technique to increase the resolution of multispectral data using a single panchromatic band with better spatial resolution – is becoming increasingly relevant not only because it can overcome resolution trade-offs that limit the utility of any one particular data source, but also because the necessary VHR data are become more freely available. On the other hand, data fusion techniques like the one employed here remain a straightforward and valuable alternative to more complex pixel-based approaches, particularly as new methods and more automated approaches are adopted for remote sensing applications. Combining multiple data sources is also advantageous given the heterogeneity of urban land and urban growth. Depending on the built-up density, building materials, and amounts/types of vegetative cover, urban areas may resemble other land cover classes more so than they

resemble one another. By tackling the classification problem from multiple domains, it is possible to isolate a large number of unique urban signatures in a relatively short amount of time.

Reduce confusion by limiting the study space. Urban areas account for a very small amount of total global land area, and land cover change within/near these areas occurs infrequently. While the exact patterns and extents of urban areas are not well-known globally, their central locations are captured in a variety of public/private databases, including point datasets, city lists, and even online mapping engines. Using very liberal buffers (up to 100 km) applied to a synthesis of these datasets (Table 1), we harnessed this information to eliminate 50% of the land extent from the image processing stream, in turn reducing the overall image processing time substantially. This approach allowed these data to be exploited without using them explicitly during image processing, thereby limiting the propagation of errors into the final results. Basing the change detection methodology on the same premise of constraining the area for classification and change detection, we were able to work 'backwards' from 2010 to map expansion for the 2000-2010 period.

The emerging digital landscape is providing vast new data sources on urban processes that could be incorporated into mapping methodologies. Data from location-based social networks (e.g. Foursquare) or geo-located internet/social media posts (e.g. Twitter, Facebook, FlickR) are increasingly being exploited to monitor and map disease outbreaks (Signorini et al., 2011) and natural disasters (Gao et al., 2011; Yates & Paquette, 2011). While the quality and reliability of crowd-sourced and volunteered geographic information

must be considered, these datasets provide opportunities for innovation in using humans as sensors.

Definitions of urban land and urban expansion are a critical component of any urban mapping methodology. Perhaps more than any other land cover type, urban area mapping is complicated not only by the juxtaposition of human constructed and natural elements, but also by a lack of consensus on how to define urban areas. In addition to satellite information, definitions may include census/population density information, economic indicators, functional boundaries (e.g. a commuter-shed), or administrative boundaries. Definitions based on physical land surface properties are a logical choice for applications using optical remote sensing data, simply because spectral and temporal properties of urban surfaces can be aligned to radiometric values in the imagery.

Past efforts have shown how varying urban definitions can lead to vastly different maps of cities and settlements (Potere et al., 2007). Our results here indicate that the definition of urban remains problematic, despite the use of consistent, high quality optical remote sensing data and a clearly established conceptual framework on urban areas. Specifically, the accuracy assessment results revealed that the majority of errors in the change detection could be traced back to definitional issues. This is likely the result of differences in labeling techniques between analysts as training data were compiled, as it can be difficult to visually and objectively estimate a 50% density threshold. However, this result does have two positive implications. First, it may be less problematic to mislabel an area that moves from 10 to 40% built up land as urban expansion, than it is to mislabel a barren area as urban expansion. Since more than a third of all error is related to definitions

instead of categorical error, the map quality may be better than reported. Second, the fact that these more subtle changes in land cover are being detected shows that the method may have potential to map land modifications (e.g. redevelopment, increases in density) in addition to land conversions.

Urban growth has increased in scope, scale, and complexity in recent decades, and has become one of the most important challenges of the 21st century. Looking forward, this research provides a tested methodology to map urban land expansion at continental to global scales using MODIS data, which can be extended to map other regions as well. Since the change detection component of this work is mostly scale-independent, this framework could be extended to map urban areas with more spatially-detailed data as well. The rise of big data and social media, along with advances in data mining and processing capacities also present opportunities to expand this framework. Potential extensions to differentiate between different built-up densities (e.g. urban core vs. low density urban) and track urban redevelopment are also promising. The high rates of urbanization characterizing many parts of East Asia have resulted in increased demand for timely land information for researchers, land use managers, governing institutions and the private sector. To this end, this work provides an up-to-date, consistent, and spatially-explicit dataset on urban extent and expansion for this rapidly evolving region.

REFERENCES

Alcantara, C., Kuemmerle, T., Baumann, M., Bragina, E. V, Griffiths, P., Hostert, P., Knorn, J., Müller, D., Prishchepov, A.V., Schierhorn, F., Sieber, A., and Radeloff, V. C. (2013). Mapping the extent of abandoned farmland in Central and Eastern Europe using MODIS time series satellite data. *Environmental Research Letters*, *8*(3), 035035. doi:10.1088/1748-9326/8/3/035035

An, K., Zhang, J. S., & Xiao, Y. (2007). Object-oriented urban dynamic monitoring - A case study of Haidian district of Beijing. *Chinese Geographical Science, 17*, 236-242.

Angel, S., Sheppard, S. C., Civco, D. L., Buckley, R., Chabaeva, A., Gitlin, L., Kraley, A., Parent, J., & Perlin, M. (2005). The dynamics of global urban expansion. *Transport and Urban Development Department Report*, Washington DC: World Bank Publications.

Alberti, M. (2005). The effects of urban patterns on ecosystem function. *International Regional Science Review, 28*, 168-192.

Avellan, T., Meier, J., & Mauser, W. (2012). Are urban areas endangering the availability of rainfed crop suitable land? *Remote Sensing Letters*, *3*(7), 631-638.

Bartholome, E., & Belward, A. S. (2005). GLC2000: A new approach to global land cover mapping from Earth observation data. *International Journal of Remote Sensing*, *26*, 1959-1977.

Belward, A. S., & Loveland, T. (1997). The IGBP-DIS global 1 km land cover data set, DISCover: First results. *International Journal of Remote Sensing*, *18*, 3291-3295.

Bhaduri, B., Bright, E., Coleman, P., & Dobson, J. (2002). LandScan: Locating people is what matters. *Geoinfomatics, 5*, 34-37.

Bhaskaran, S., Paramananda, S., & Ramnarayan, M. (2010). Per-pixel and object-oriented classification methods for mapping urban features using Ikonos satellite data. *Applied Geography*, *30*(4), 650–665.

Borak, J. S., Lambin, E. F., & Strahler, a. H. (2000). The use of temporal metrics for land cover change detection at coarse spatial scales. *International Journal of Remote Sensing*, *21*(6-7), 1415–1432. doi:10.1080/014311600210245

Bradley, B. A., Jacob, R. W., Hermance, J. F., & Mustard, J. F. (2007). A curve fitting procedure to derive inter-annual phenologies from time series of noisy satellite NDVI data. *Remote Sensing of Environment*, *106*, 137–145.

Carrion-Flores, C., & Irwin, E. (2004). Determinants of residential land-use conversion and sprawl at the rural-urban fringe. *American Journal of Agricultural Economics*, *86*(November), 889-904.

Chen, X., & Nordhaus, W.D. (2011). Using luminosity data as a proxy for economic statistics. *Proceedings of the National Academy of Sciences USA, 108*, 8589-8594.

Center for International Earth Science Information Network (CIESIN). (2004). *Global Rural–Urban Mapping Project (GRUMP)*, Alpha Version: Urban Extents. (available on-line at: http://sedac.ciesin.columbia.edu/gpw).

Cihlar, J. (2000). Land cover mapping of large areas from satellites: Status and research priorities. *International Journal of Remote Sensing*, *21*(6-7), 1093–1114. doi:10.1080/014311600210092

Clark, M. L., Aide, T. M., Grau, H. R., & Riner, G. (2010). A scalable approach to mapping annual land cover at 250 m using MODIS time series data: A case study in the Dry Chaco ecoregion of South America. *Remote Sensing of Environment*, *114*(11), 2816–2832. doi:10.1016/j.rse.2010.07.001

Clark, M. L., Aide, T. M., & Riner, G. (2012). Land change for all municipalities in Latin America and the Caribbean assessed from 250-m MODIS imagery (2001–2010). *Remote Sensing of Environment*, *126*, 84–103. doi:10.1016/j.rse.2012.08.013

Corbane, C., Faure, J.-F., Baghdadi, N., Villeneuve, N., & Petit, M. (2008). Rapid Urban Mapping Using SAR/Optical Imagery Synergy. *Sensors*, *8*(11), 7125–7143. doi:10.3390/s8117125

Deichmann, U., & Yetman, G. (2001). Transforming Population Data for Interdisciplinary Usages : From census to grid, (October).

Deng, J. S., Wang, K., Li, J., & Deng, Y. H. (2009). Urban land use change detection using multisensor satellite images. *Pedosphere*, *19*(1), 96-103. doi:10.1016/S1002-0160(08)60088-0.

Deuskar, C., Schneider, A., & Dastur, A. (in review, 2014). *Mapping a decade of urban change: East Asia, 2000-2010*. World Bank Publications, Washington DC, USA.

Elvidge, C., Tuttle, B. T., Sutton, P. C., Baugh,K. E., Howard,A. T., Milesi, C., Bhaduri, B. L., & Nemani, R. (2007). Global distribution and density of constructed impervious surfaces. *Sensors*, *7*, 1962-1979.

Elvidge, C.D., Sutton, P., Ghosh, T., Tuttle, B., Baugh, K., Bhaduri, B., & Bright, E. (2009). A global poverty map derived from satellite data. *Computers & GISciences*, *35*, 1652-1660.

European Space Agency (ESA). (2008). *GlobCover products description and validation report* (available online at: ftp://uranus.esrin.esa.int/pub/globcover_v2/global/GLOBCOVER_Products_Description_Validation_Report_I2.1.pdf).

Friedl, M. A., & Brodley, C. E. (1997). Decision tree classification of land cover from remotely sensed data. *Remote Sensing of Environment*, *61*, 399–409.

Friedl, M. A., McIver, D. K., Hodges, J., Zhang, X., Muchoney, D., Strahler, A., Woodcock, C. E., Gopal, S., Schneider, A., Cooper, A., Baccini, A., Gao, F., & Schaaf, C. (2002). Global land cover mapping from MODIS: Algorithms and early results. *Remote Sensing of Environment*, *83*, 287–302.

Friedl, M. A., Sulla-Menashe, D., Tan, B., Schneider, A., Ramankutty, N., Sibley, A., & Huang, X. (2010). MODIS Collection 5 global land cover: Algorithm refinements and characterization of new datasets. *Remote Sensing of Environment*, *114*, 168–182.

Gamba, P., & Herold, M. (Eds.). (2009*). Global mapping of human settlements: Experiences, datasets, and prospects*. Boca Raton, Florida, USA, CRC Press.

Gao, F., Morisette, J. T., Wolfe, R. E., Ederer, G., Pedelty, J., Masuoka, E., Myneni, R., Tan, B., & Nightingale, J. (2008). An algorithm to produce temporally and spatially continuous MODIS-LAI time series. *IEEE Transactions in Geoscience and Remote Sensing*, *5*, 60-64.

Gao, H., Barbier, G., & Goolsby, R. (2011). Harnessing the Crowdsourcing Power of Social Media for Disaster Relief. *IEEE Intelligent Systems*, *26*(3), 10–14. doi:10.1109/MIS.2011.52

Geerken, R. a. (2009). An algorithm to classify and monitor seasonal variations in vegetation phenologies and their inter-annual change. *ISPRS Journal of Photogrammetry and Remote Sensing*, *64*(4), 422–431. doi:10.1016/j.isprsjprs.2009.03.001

Ghimire, B., Rogan, J., & Miller, J. (2010). Contextual land-cover classification: incorporating spatial dependence in land-cover classification models using random forests and the Getis statistic. *Remote Sensing Letters*, *1*(1), 45–54. doi:10.1080/01431160903252327

Goldewijk, K. (2005). Three centuries of global population growth: A spatially referenced population density database for 1700–2000. *Population and Environment*, *26*, 343-367.

Griffiths, P., Hostert, P., Gruebner, O., & Van der Linden, S. (2010). Mapping megacity growth with multi-sensor data. *Remote Sensing of Environment*, *114*, 426–439.

Grimm, N. B., Foster, D., Groffman, P., Grove, J. M., Hopkinson, C. S., Nadelhoffer, K. J., Pataki, D. E., & Peters, D. P. C. (2008). The changing landscape: ecosystem responses to

urbanization and pollution across climatic and societal gradients. *Frontiers in Ecology and the Environment, 6*, 264-272.

Gueneralp, B., & Seto, K. C. (2013). Futures of global urban expansion: uncertainties and implications for biodiversity conservation. *Environmental Research Letters, 8*(1), 014025 (article).

Hansen, M.C., Potapov, P.V., Moore, R., Hancher, M., Turubanova, A., Tyukavina, A., Thau, D., Stehman, S., Goetz, S.J., Loveland, T.R., Kommareddy, A., Egorov, A., Chini, L., Justice, C., Townshend, J.R.G. (2013). High-resolution global maps of 21st century forest cover change. *Science, 342,* 850-853.

Hansen, M. C., Townshend, J. R. G., Defries, R. S., & Carroll, M. (2005). Estimation of tree cover using MODIS data at global, continental and regional/local scales. *International Journal of Remote Sensing, 26*, 4359–4380.

Herold, M., Scepan, J., & Clarke, K. C. (2002). The use of remote sensing and landscape metrics to describe structures and changes in urban land uses. *Environment and Planning A, 34*(8), 1443–1458. doi:10.1068/a3496.

Hilker, T., Wulder, M. A., Coops, N. C., Linke, J., McDermid, G., Masek, J. G., Gao, F., & White, J. C. (2009). A new data fusion model for high spatial- and temporal-resolution mapping of forest disturbance based on Landsat and MODIS. *Remote Sensing of Environment, 113*, 1613-1627.

Homer, C., Huang, C., Yang, L., Wylie, B., & Coan, M. (2004). Development of a 2001 National Land-Cover Database for the United States. *Photogrammetric Engineering and Remote Sensing, 70*, 829-840.
Howarth, P. J., & Boasson, E. (1983). Landsat digital enhancements for change detection in urban environments. *Remote Sensing of Environment, 13,* 149-160.

Jakubauskas, M. E., Legates, D. R., & Kastens, J. H. (2001). Harmonic Analysis of Time-Series AVHRR NDVI Data, *67*(4), 461–470.

Jensen, J. R., & Cowen, D. C. (1999). Remote sensing of urban/suburban infrastructure and socioeconomic attributes. *Photogrammetric Engineering and Remote Sensing*, 65, 611-622.

Jensen, J. R., & Toll, D. L. (1982). Detecting residential land use development at the urban fringe. *Photogrammetric Engineering and Remote Sensing*, *48*, 629-643.

Jones, B., & O'Neill, B. C. (2013). Historically grounded spatial population projections for the continental United States. *Environmental Research Letters, 8*(4), 044021 (article).

Kasimu, A., Tateishi, R., & Hoan, N. T. (2009). Global urban characterization using population density, DMSP and MODIS data. *2009 Joint Urban Remote Sensing Event*, 1–7. doi:10.1109/URS.2009.5137493

Kennedy, R.E., Andrefouet, S., Cohen, W.B., Gomez, C., Griffiths, P., Hais, M., Healey, S.P., Helmer, E.H., Hostert, P., Lyons, M., Meigs, G., Pflugmacher, D., Phinn, S., Powell, S.L., Scarth, P., Schroeder, T.A., Schneider, A., Sen, S., Sonnenschein, R., Vogelmann, J.E., Wulder, M.A., & Zhu, Z. (2014). Bringing an ecological view of change to Landsat-based remote sensing. *Frontiers in Ecology*, in press.

Kennedy, R. E., Cohen, W. B., & Schroeder, T. A. (2007). Trajectory-based change detection for automated characterization of forest disturbance dynamics. *Remote Sensing of Environment, 110,* 370-386.

Kontgis, C. P., Schneider, A., Fox, J., Saksena, S., Spencer, J., Castrence, M. Monitoring peri-urbanization in the greater Ho Chi Minh City metropolitan area. Journal of Applied Geography, under review.

Kuemmerle, T., Chaskovskyy, O., Knorn, J., Radeloff, V. C., Kruhlov, I., Keeton, W. S., & Hostert, P. (2009). Forest cover change and illegal logging in the Ukrainian Carpathians in the transition period from 1988 to 2007. *Remote Sensing of Environment, 113,* 1194-1207.

Lambin, E.F., & Meyfroidt, P. (2011). Global land use change, economic globalization, and the looming land scarcity. *Proceedings of the National Academy of Sciences USA, 108,* 3465-3472.

Leinenkugel, P., Kuenzer, C., & Dech, S. (2013). Comparison and enhancement of MODIS cloud mask products for Southeast Asia. *International Journal of Remote Sensing*, *34*(8), 2730–2748. doi:10.1080/01431161.2012.750037

Linderman, M., Rowhani, P., Benz, D., Serneels, S., & Lambin, E. F. (2005). Land-cover change and vegetation dynamics across Africa. *Journal of Geophysical Research-Atmospheres*, *110*(D12), D12104 (article).

Loveland, T., Zhu, Z., Ohlen, D., Brown, J., Reed, B., & Yang, L. (1999). An analysis of the IGBP global land cover characterization process. *Photogrammetric Engineering and Remote Sensing*, *65*, 1021-1031.

Martin, L., & Howarth, P. (1989). Change-detection accuracy assessment using SPOT multispectral imagery of the rural-urban fringe. *Remote Sensing of Environment*, *30*(1), 55–66. doi:10.1016/0034-4257(89)90047-3.

Martínez, B., & Gilabert, M. A. (2009). Vegetation dynamics from NDVI time series analysis using the wavelet transform. *Remote Sensing of Environment*, *113*(9), 1823–1842. doi:10.1016/j.rse.2009.04.016

Masek, J. G., Huang, C., Wolfe, R., Cohen, W., Hall, F., Kutler, J., & Nelson, P. (2008). North American forest disturbance mapped from a decadal Landsat record. *Remote Sensing of Environment*, *112*(6), 2914–2926. doi:10.1016/j.rse.2008.02.010

McDonald, R. I., Green, P., Balk, D., Fekete, B. M., Revenga, C., Todd, M., & Montgomery, M. (2011). Urban growth, climate change, and freshwater availability. *Proceedings of the National Academy of Sciences of the United States of America*, *108*(15), 6312-6317.

McGrane, S. J., Tetzlaff, D., & Soulsby, C. (2014). Influence of lowland aquifers and anthropogenic impacts on the isotope hydrology of contrasting mesoscale catchments. *Hydrological Processes*, *28*(3), 793-808.

McIver, D.K., & Friedl, M. A. (2001). Estimating pixel-scale land cover classification confidence using non-parametric machine learning methods. *IEEE Transactions on Geoscience and Remote Sensing*, *39*, 1959–1968.

MDA Federal (2004). *Landsat GeoCover Maps.* Washington, DC (available online at: http://www.mdafederal.com/geocover/geocoverlc/).

NGDC (National Geophysical Data Center). (2007). Nighttime Lights data. Available online at http://ngdc.noaa.gov/eog/dmsp.html (accessed 10 April 2013).

Nordbo, A., Jarvi, L., Haapanala, S., Wood, C. R., & Vesala, T. (2012). Fraction of natural area as main predictor of net CO2 emissions from cities. *Geophysical Research Letters*, *39*, L20802 (article).

Oleson, K. W., Bonan, G. B., Feddema, J., Vertenstein, M., & Grimmond, C. S. B. (2008). An urban parameterization for a global climate model: 1. Formulation and evaluation for two cities. *Journal of Applied Meteorology and Climatology*, *47*, 1038-1060.

Olson, D. M., Dinerstein, E., Wikramanayake, E., Burgess, N., Powell, G., Underwood, E., et al. (2001). Terrestrial ecoregions of the world: A new map of life on Earth. *BioScience, 51*, 933-938.

Pacifici, F., Chini, M., & Emery, W. J. (2009). A neural network approach using multi-scale textural metrics from very high-resolution panchromatic imagery for urban land-use classification. *Remote Sensing of Environment*, *113*(6), 1276–1292. doi:10.1016/j.rse.2009.02.014

Pesaresi, M. (2000). Texture Analysis for Urban Pattern Recognition Using Fine-resolution Panchromatic Satellite Imagery, *4*(1), 43–63.

Potere, D., & Schneider, A. (2007). A critical look at representations of urban areas in global maps. *GeoJournal*, *69*, 55-80.

Potere, D., Schneider, A., Schlomo, A., & Civco, D. A. (2009). Mapping urban areas on a global scale: Which of the eight maps now available is more accurate? *International Journal of Remote Sensing*, *30*, 6531-6558.

Quinlan, J. R. (1993). *C4.5: Programs for machine learning*. New York: Morgan Kaufmann Publishers.

Radeloff, V. C., Hammer, R. B., Stewart, S. I., Fried, J. S., Holcomb, S. S., & McKeefry, J. F. (2005). The wildland-urban interface in the United States. *Ecological Applications*, *15*(3), 799-805.

Rahman, A. F., Dragoni, D., Didan, K., Barreto-Munoz, A., & Hutabarat, J. a. (2013). Detecting large scale conversion of mangroves to aquaculture with change point and mixed-pixel analyses of high-fidelity MODIS data. *Remote Sensing of Environment*, *130*, 96–107. doi:10.1016/j.rse.2012.11.014

Ridd, M. K., & Liu, J. (1998). A comparison of four algorithms for change detection in an urban environment. *Remote Sensing of Environment*, *63*(2), 95-100.

Sakamoto, T., Nguyen, N. V., Kotera, A., Ohno, H., Ishitsuka, N., & Yokozawa, M. (2007). Detecting temporal changes in the extent of annual flooding within the Cambodia and the Vietnamese Mekong Delta from MODIS time-series imagery. *Remote Sensing of Environment*, *109*, 295-313.

Sanli, F. B., Kurucu, Y., & Esetlili, M. T. (2009). Determining land use changes by radar-optic fused images and monitoring its environmental impacts in Edremit region of western Turkey. *Environmental Monitoring and Assessment*, *151*, 45-58.

Sahr, K., White, D., & Kimerling, A. J. (2003). Geodesic discrete global grid systems. *Cartography and Geographic Information Science*, *30*(2), 121-134. doi:10.1559/152304003100011090.

Schaaf, C. B., Gao, F., Strahler, A. H., Lucht, W., Li, X., Tsang, T., Strugnell, N. C., Zhang, X., Jin, Y., Muller, J. P., Lewis, P., Barnsley, M., Hobson, P., Disney, M., Roberts, G., Dunderdale, M., Doll, C., d'Entremont, R. P., Hu, B., Liang, S., Privette, J. L., & Roy, D. (2002). First operational BRDF, albedo nadir reflectance products from MODIS. *Remote Sensing of Environment*, *83*, 135-148.

Schneider, A. (2012). Monitoring land cover change in urban and peri-urban areas using dense time stacks of Landsat satellite data and a data mining approach. *Remote Sensing of Environment*, *124*, 689-704.

Schneider, A., Friedl, M. A., Mciver, D. K., & Woodcock, C. E. (2003). Mapping urban areas by fusing multiple sources of coarse resolution remotely sensed data. *Photogrammetric Engineering and Remote Sensing, 69,* 1377-1386.

Schneider, A., Friedl, M. A., & Potere, D. (2009). A new map of global urban extent from MODIS satellite data. *Environmental Research Letters, 4,* 044003 (article).

Schneider, A., Friedl, M. A., & Potere, D. (2010). Mapping urban areas globally using MODIS 500m data: New methods and datasets based on urban ecoregions. *Remote Sensing of Environment, 114,* 1733-1746.

Schneider, A., & Woodcock, C. E. (2008). Compact, dispersed, fragmented, extensive? A comparison of urban expansion in twenty-five global cities using remotely sensed data, pattern metrics and census information. *Urban Studies, 45,* 659-692.

Scott, A. J., Carter, C., Reed, M. R., Larkham, P., Adams, D., Morton, N., Waters, R., Collier, D., Crean, C., Curzon, R., Forster, R., Gibbs, P., Grayson, N., Hardman, M., Hearle, A., Jarvis, D., Kennet, M., Leach, K., Middleton, M., Schiessel, N., Stonyer, B., & Coles, R. (2013). Disintegrated development at the rural-urban fringe: Re-connecting spatial planning theory and practice. *Progress in Planning, 83,* 1-52.

Shaban, M.A. & Dikshit O. (2001). Improvement of classification in urban areas by the use of textural features: the case study of Lucknow city, Uttar Pradesh. *International Journal of Remote Sensing, 22,* 565-593.

Seto, K. C., Sanchez-Rodriguez, R., & Fragkias, M. (2010). The new geography of contemporary urbanization and the environment. *Annual Review of Environment and Resources, 35,* 167-194.

Seto, K. C., Fragkias, M., Güneralp, B., & Reilly, M. K. (2011). A meta-analysis of global urban land expansion. *PLoS One, 6,* e23777 (article).

Signorini, A., Segre, A. M., & Polgreen, P. M. (2011). The use of Twitter to track levels of disease activity and public concern in the U.S. during the influenza A H1N1 pandemic. *PloS One, 6*(5), e19467. doi:10.1371/journal.pone.0019467

Stefanov, W. L., Ramsey, M. S., & Christensen, P. R. (2001). Monitoring urban land cover change: An expert system approach to land cover classification of semiarid to arid urban centers. *Remote Sensing of Environment, 77,* 173-185.

Tan, B., Morisette, J. T., Wolfe, R. E., Feng, G., Ederer, G. A., Nightingale, J., & Pedelty, J. A. (2011). An enhanced TIMESAT algorithm for estimating vegetation phenology metrics from MODIS data. *IEEE Journal of Selected Topics in Applied Earth Observations, 4,* 361-371.

Tan, M., Li, X., Xie, H., & Lu, C. (2005). Urban land expansion and arable land loss in China—a case study of Beijing–Tianjin–Hebei region. *Land Use Policy*, *22*(3), 187-196. doi:10.1016/j.landusepol.2004.03.003.

Tatem, A. J., Noor, A. M., von Hagen, C., Di Gregorio, A., & Hay, S. I. (2007). High resolution settlement and population maps for low income nations: combining land cover and national census in East Africa. *PLoS One 2*, e1298 (article).

Taubenböck, H., Esch, T., Felbier, a., Wiesner, M., Roth, a., & Dech, S. (2012). Monitoring urbanization in mega cities from space. *Remote Sensing of Environment*, *117*, 162–176. doi:10.1016/j.rse.2011.09.015

Verbesselt, J., Hyndman, R., Newnham, G., & Culvenor, D. (2010). Detecting trend and seasonal changes in satellite image time series. *Remote Sensing of Environment*, *114*(1), 106-115. doi:10.1016/j.rse.2009.08.014.

Wang, L., Li, C., Ying, Q., Cheng, X., Wang, X., Li, X., Hu, L., Liang, L., Yu, L., Huang, H., & Gong, P. (2012). China's urban expansion from 1990 to 2010 determined with satellite remote sensing. *Chinese Science Bulletin*, *57*, 2802-2812.

Weng, Q. (2001). A remote sensing-GIS evaluation of urban expansion and its impact on surface temperature in the Zhujiang Delta China. *International Journal of Remote Sensing*, *22*, 1999-2014.

Wentz, E. a., Stefanov, W. L., Gries, C., & Hope, D. (2006). Land use and land cover mapping from diverse data sources for an arid urban environments. *Computers, Environment and Urban Systems*, *30*(3), 320–346. doi:10.1016/j.compenvurbsys.2004.07.002

Wilhelmi, O., de Sherbinin, A., & Hayden, M. (2013). Exposure to heat stress in urban environments. King, B., & Crews, K. A. (eds). *Ecologies and Politics of Health Book Series*, Routledge Studies in Human Geography, 41, 219-238.

Xin, Q., Olofsson, P., Zhe, Z., Tan, B., & Woodcock, C. (2013). Toward near real-time monitoring of forest disturbance by fusion of MODIS and Landsat data. *Remote Sensing of Environment*, *135*, 234-247.

Yates, D., & Paquette, S. (2011). Emergency knowledge management and social media technologies: A case study of the 2010 Haitian earthquake. *International Journal of Information Management*, *31*(1), 6–13. doi:10.1016/j.ijinfomgt.2010.10.001

Yuan, F., Sawaya, K. E., Loeffelholz, B. C., & Bauer, M. E. (2005). Land cover classification and change analysis of the Twin Cities (Minnesota) Metropolitan Area by

multitemporal Landsat remote sensing. *Remote Sensing of Environment*, *98*(2-3), 317-328. doi:10.1016/j.rse.2005.08.006.

Zhang, Q., Wang, J., Peng, X., Gong, P., & Shi, P. (2002). Urban built-up land change detection with road density and spectral information from multi-temporal Landsat TM data. *International Journal of Remote Sensing, 23,* 3057-3078.

Zhang, X. Y., Friedl, M. A., Schaaf, C. B., Strahler, A. H., Hodges, J. C. F., Gao, F., Reed, B. C., & Huete, A. (2003). Monitoring vegetation phenology using MODIS. *Remote Sensing of Environment*, *84*(3), 471-475, PII S0034-4257(02)00135-9 (article).

Zhao, S., Zhu, C., Zhou, D., Huang, D., Werner, J. (2013). Organic carbon storage in China's urban areas. *PLoS One*, *8*(8), e71975 (article).

Zhou, L., Dickinson, R. E., Tian, Y., Fang, J., Li, Q., Kaufmann, R., Tucker, C., & Myneni, R. (2004). Evidence for a significant urbanization effect on climate in China. *Proceedings of the National Academy of Sciences of the United States of America*, *101*(26), 9540-9544.

Zhu, Z., Woodcock, C. E., & Olofsson, P. (2012). Continuous monitoring of forest disturbance using all available Landsat imagery. *Remote Sensing of Environment*, *122*, 75–91. doi:10.1016/j.rse.2011.10.030

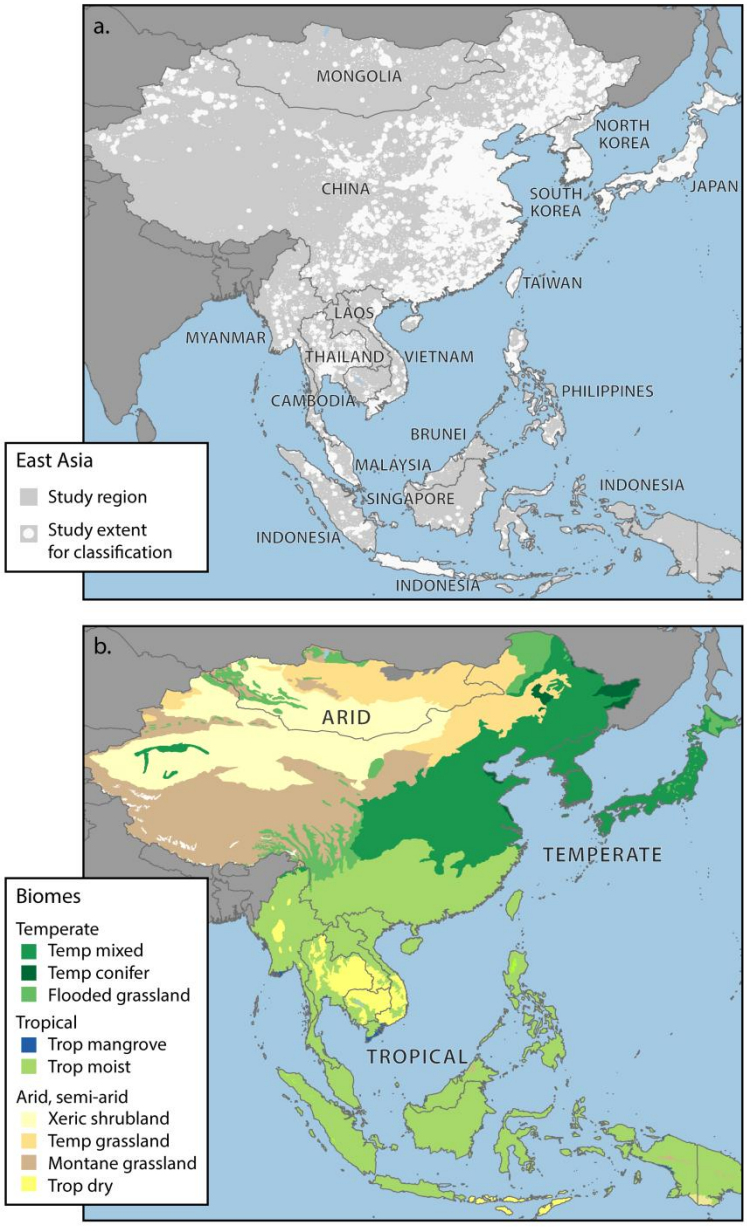

Figure 1. Maps of the East Asia region illustrating (a) the study area extent defined by known locations of urban land, and (b) Olson's biome designation, used to delineate areas of similar ecoclimatic characteristics for data processing.

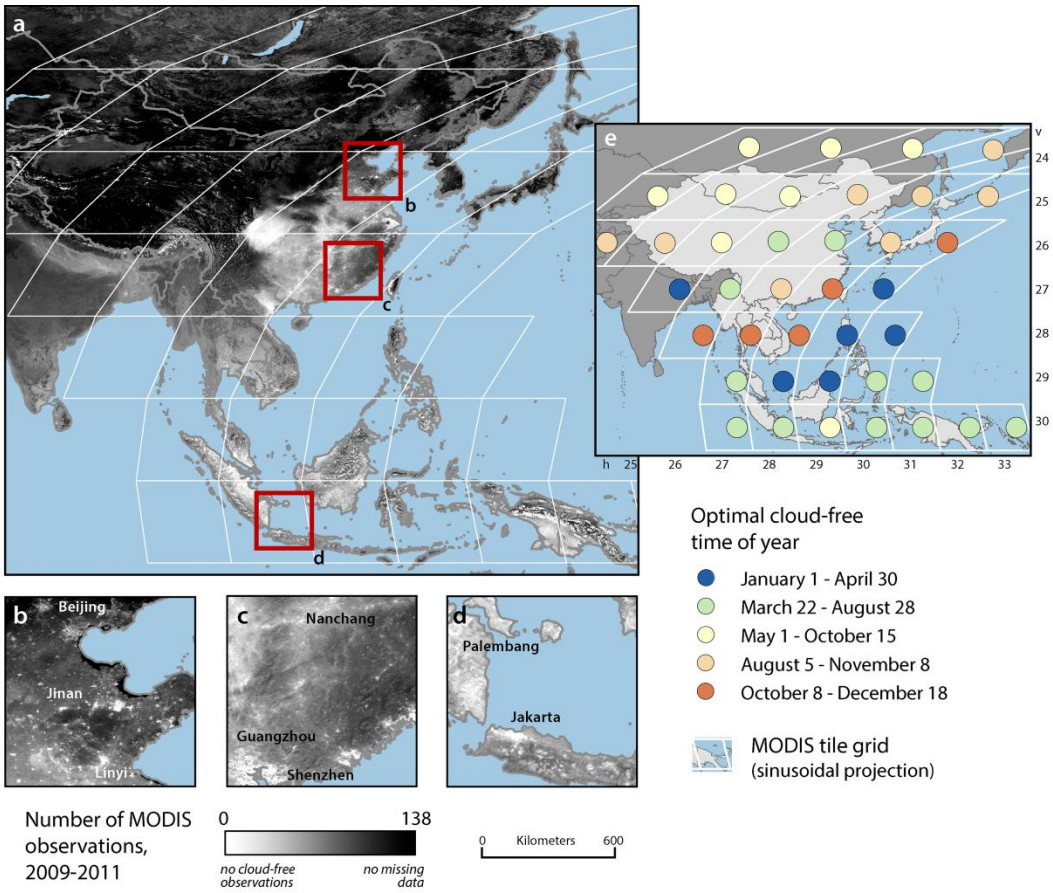

Figure 2. The distribution of missing data observations in the MODIS 500 m NBAR data for (a) the East Asia study region, and for (b) northeastern China, (c) southeastern China, and (d) central Indonesia. Note the small number of cloud-free observations in cities and tropical/subtropical areas. Panel (e) illustrates the results of the optimization algorithm used to select the cloud-free time of year for each tile.

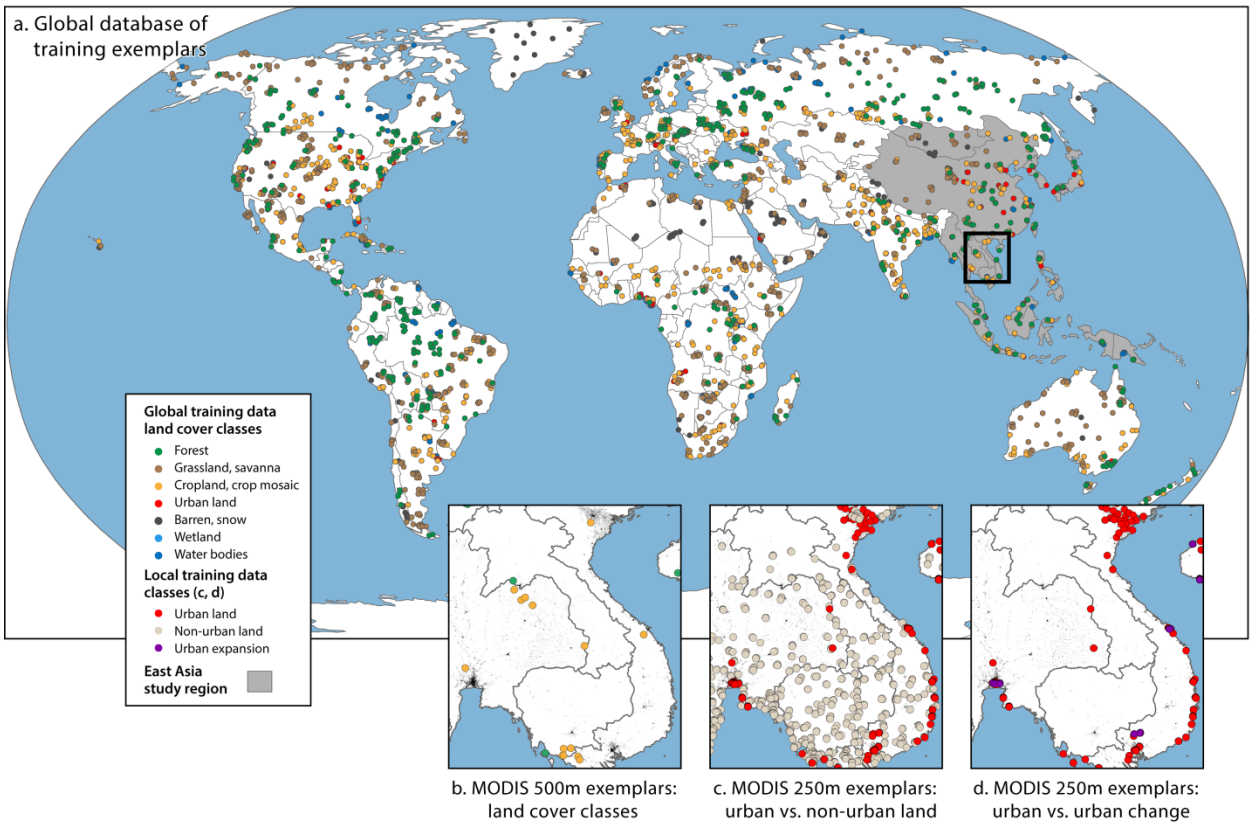

Figure 3. Global (a) and local views (b-d) of the three training datasets compiled for this research. To classify ca 2010 urban land using the MODIS 500 m data, we rely on a global distribution of >2000 training sites (Friedl et al., 2010) (a, b). This database was updated and augmented with an additional 400+ training sites in East and Southeast Asia. To create the *a priori* urban probability surface using MODIS 250 m data, we collected training data on a tile-by-tile basis for urban and non-urban areas (c). We then adapted (c) to represent stable urban land and urban expansion, 2000-2010 (d), for use in the change detection approach.

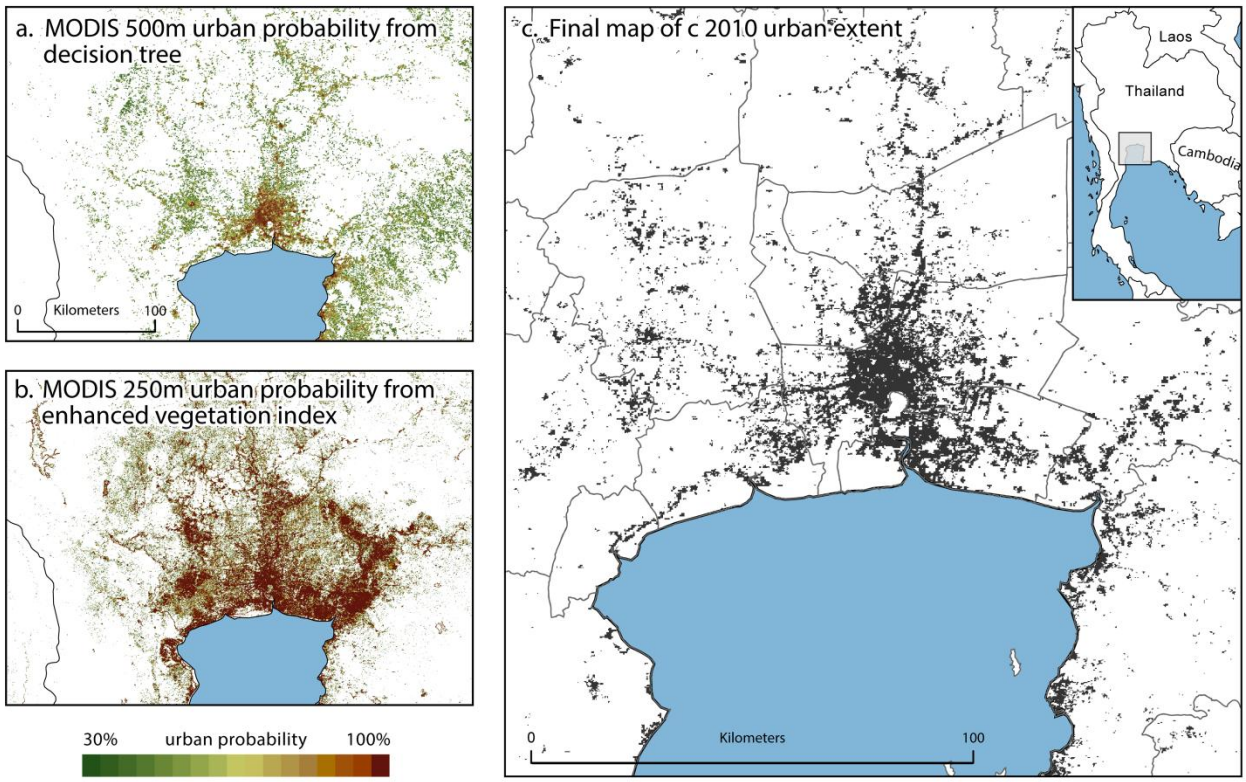

Figure 4. The data fusion approach used to map c 2010 urban extent for Bangkok, Thailand, illustrating (a) the urban class probability from the MODIS 500 m supervised decision tree classification; (b) the *a priori* surface for urban land developed from the MODIS 250 m enhanced vegetation index data; and (c) the final map of urban extent from the fusion of the (a) and (b) using Bayes' Rule.

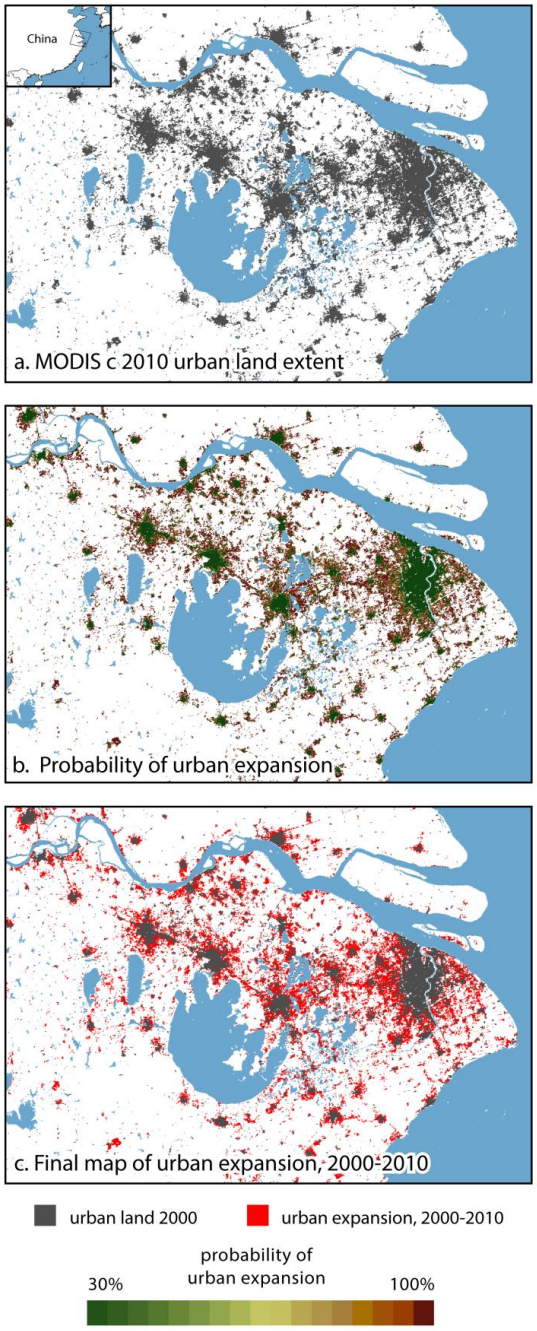

Figure 5. An illustration of the steps used to characterize urban expansion for the greater Shanghai, China, region: (a) the final map of ca 2010 urban land is used to mask the area of interest; (b) a multi-date composite change detection method is used to generate the probability of urban expansion; and (c) the final map of urban land and urban expansion, after the urban expansion probabilities have been thresholded based on visual interpretation of the probability map (b) in Google Earth.

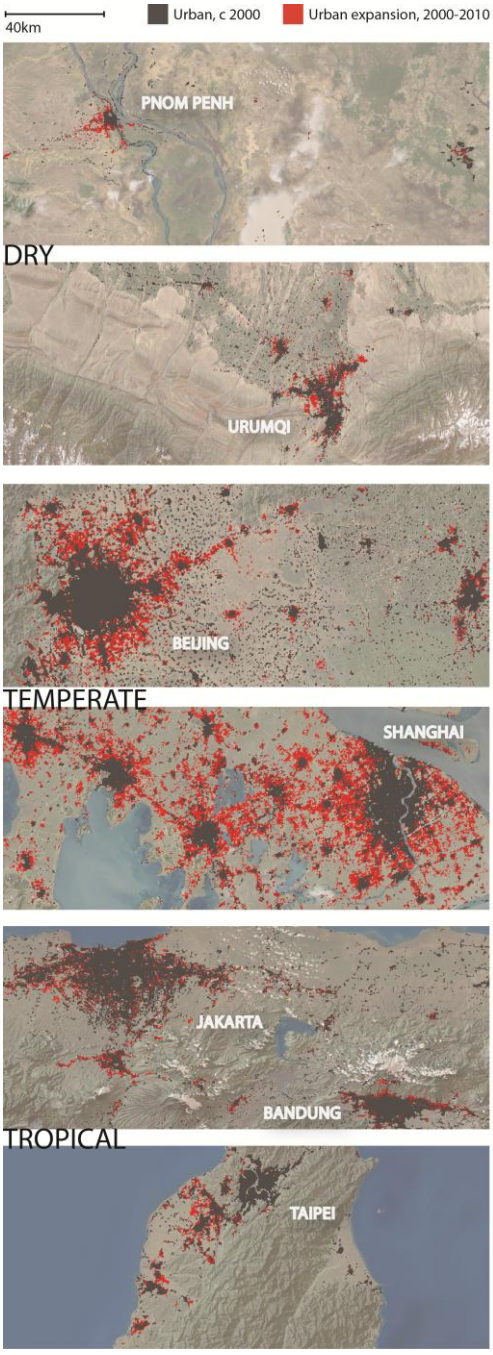

Figure 6. Urban land and urban expansion 2000-2010 in East Asia for regions spanning several countries and biomes: (a) Cambodia - tropical dry forest; (b) China - xeric/shrubland; (c) China – temperate mixed forest; (d) China – temperate mixed forest; (e) Indonesia – tropical moist forest (f) Taiwan – tropical moist forest.

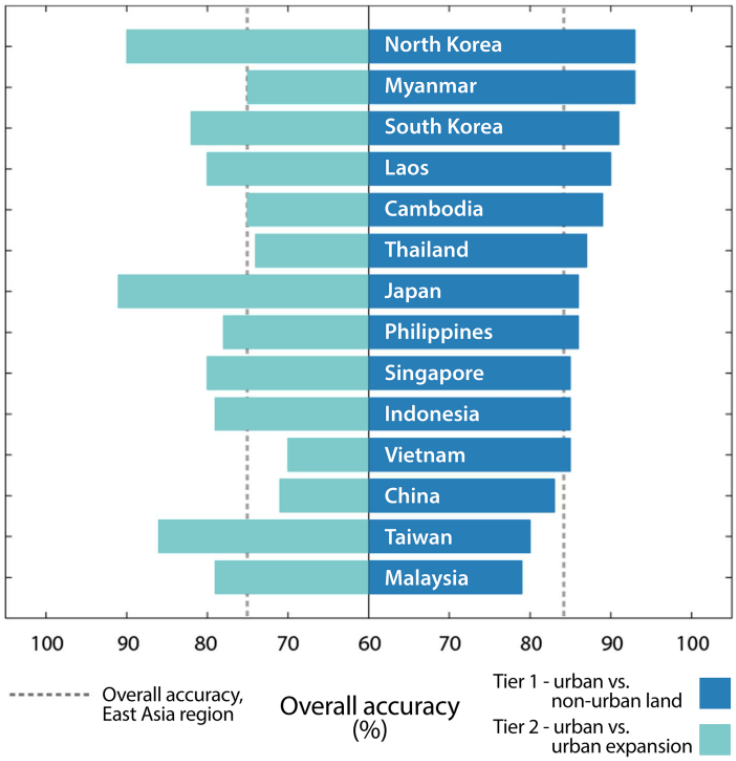

Figure 7. The overall accuracy results for the tier one and tier two assessments by country.

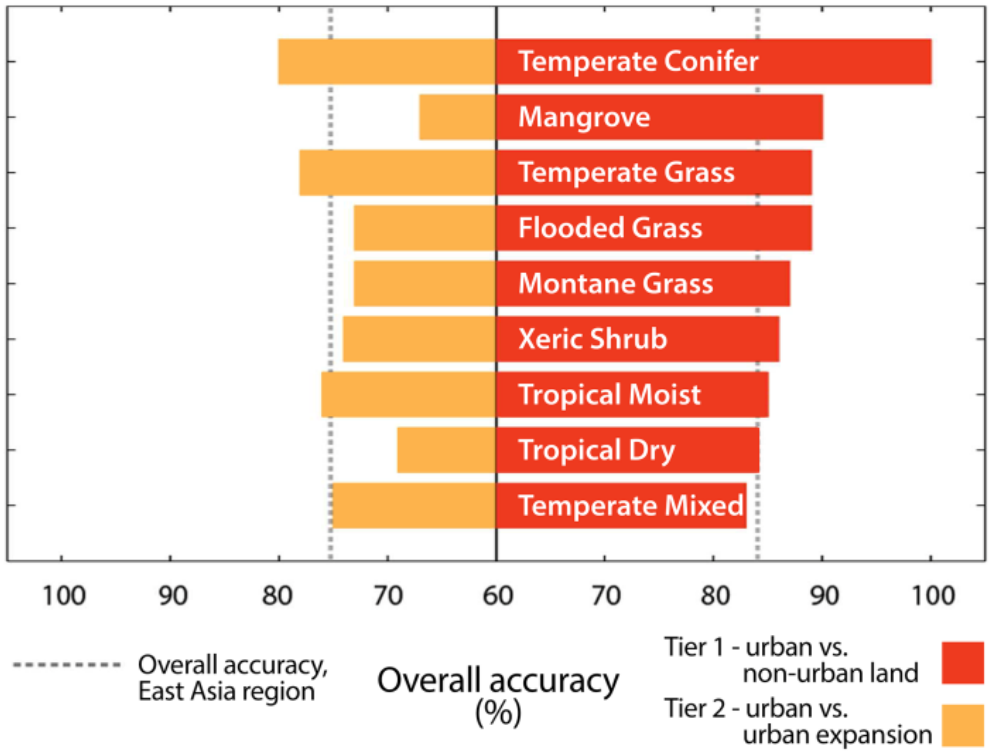

Figure 8. The overall accuracy results for the tier one and tier two assessments by biome.

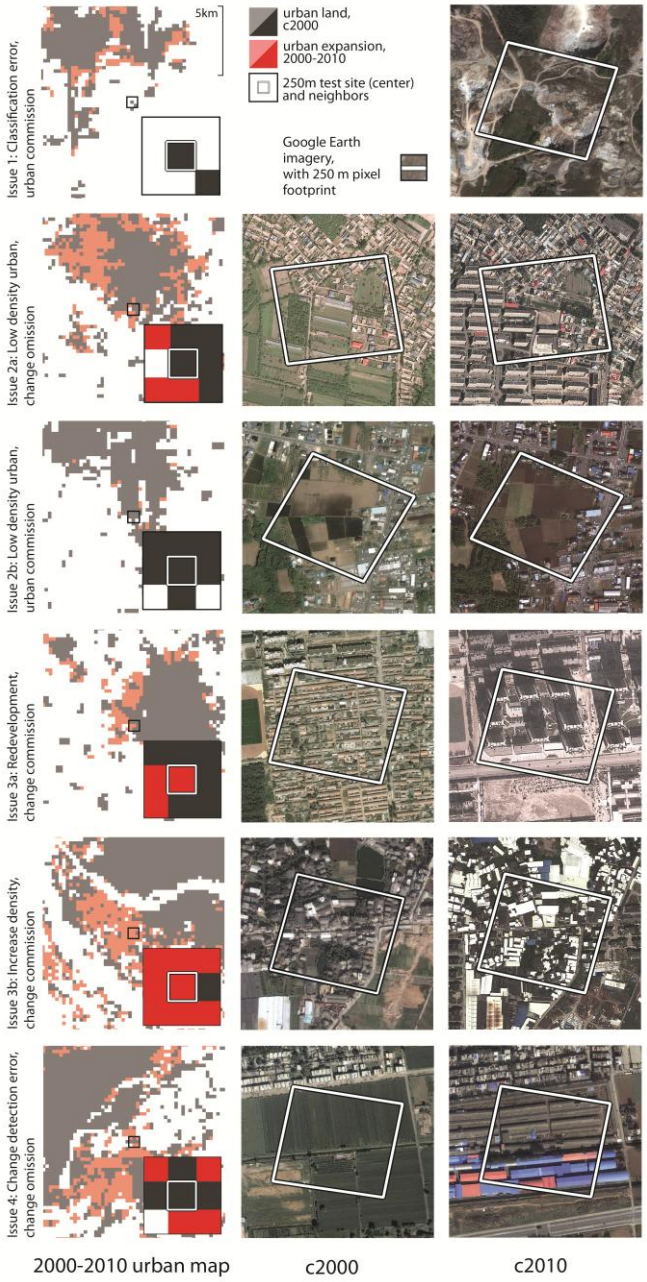

Figure 9. A sample of the types of issues associated with mislabeled sites in the tier two accuracy assessment of urban land and urban expansion (see Table 11 for full description and frequency of occurrence). The locations of the sites from top to bottom are: Dashiqiao, China; Yining City, China; Ibaraki, Japan; Langfang, China; Fuzhou, China; and Luoyang, China.

Table 1. Datasets used to define the study extent in East Asia for satellite image processing.

Dataset	Producer	Description	Location	Website or citation
MODIS 500 m map of global urban extent	University of Wisconsin-Madison	Map of 88,578 urban patches >1 km^2 used to verify, geolocate, and update city points.	Global	http://www.sage.wisc.edu
GRUMP city points	Center for International Earth Science Information Network (CIESIN), Columbia University, International Food Policy Research Institute (IFPRI), World Bank, Centro Internacional de Agricultura Tropical (CIAT)	Point dataset of 67,935 cities, towns and settlements.	Global	http://sedac.ciesin.columbia.edu
Urban agglomerations with >750,000 inhabitants, 2011	United Nations Department of Economic and Social Affairs Population Division	Point dataset of 633 cities >750,000 persons.	Global	http://esa.un.org/unup/GIS-Files/gis_1.htm
Universe of cities	Angel, Lincoln Institute of Land Policy	Point dataset of 3,943 cities >100,000 persons.	Global	Angel, S. (2012). *Planet of Cities*. Cambridge, Massachusetts, Lincoln Institute of Land Policy.
Chinese city point data	Chinese Academy of Sciences	Point dataset of 664 cities.	China	Chinese Academy of Sciences (2011). Beijing, China.
Google Earth populated places	Google Earth Pro v7.1. Layers: populated places	City point location used to verify, geolocate, and update city points.	Global	http://www.google.com/earth

Table 2. Remote sensing and training datasets used to map c 2010 urban extent and 2000-2010 urban expansion.

	Dataset	Description	Source	Location	Time period	Spatial unit
Classification c2010	MCD43A4, MCD43A2	MODIS nadir BRDF-adjusted reflectance (NBAR) and quality product 8-day composites	MODIS Land Team, Boston University	Global	Monthly composites, 2009-2011	500 m pixel
	STEP land cover database	Training exemplar database used with NBAR data	Boston University, University of Wisconsin-Madison	Global	c 2010	500 m – 2 km polygon
	MOD09Q1G EVI	MODIS Enhanced Vegetation Index (EVI) 8-day composites	NASA Goddard Space Flight Center	East Asia	Annual growing season maximum, 2009-2010	250 m pixel
	Urban, non-urban training data	Training set database used with EVI data	University of Wisconsin-Madison	East Asia	c 2010	250 m pixel
	MOD44W	MODIS land-water mask	United States Geological Survey	East Asia	c 2010	250 m pixel
Change detection 2000-2010	MOD09Q1G EVI	MODIS Enhanced Vegetation Index (EVI) 8-day composites	NASA Goddard Space Flight Center	East Asia	Annual growing season maximum, 2001-2010	250 m pixel
	Urban and urban expansion training data	Training set database used with EVI data	University of Wisconsin-Madison	East Asia	2000-2010	250 m pixel

Abbreviations: Moderate Resolution Imaging Spectroradiometer (MODIS), Bidirectional reflectance distribution function (BRDF), System for Terrestrial Ecosystem Parameterization (STEP), Enhanced Vegetation Index (EVI).

Table 3. A comparison of results from the logistic regression models used to estimate an urban / non-urban probability surface with MODIS 250 m enhanced vegetation index (EVI) data. Models were tested with (a) different explanatory variables, and (b) different methods of training data collection.

	Sample size (n)	Number of predictors (x_i)	Number of significant predictors $\alpha = 0.05$ (x_i)	Area under ROC curve
a. Predictor variables				
1 Growing season, all 8-day observations (2010)	1237	23	9	96.0
2 Growing season maximum (2009)	1237	1	1	94.6
3 Growing season maximum (2010)	1237	1	1	93.5
4 Growing season maximum (2009, 2010)	1237	2	2	98.6
5 Growing season maximum (2001, 2009, 2010)	1237	3	2	97.5
b. Method of training data collection *(using model 3)*				
6 STEP database (Google Earth imagery)	3611	1	1	79.7
7 250m pixels (MODIS imagery)	1237	1	1	93.5

Table 4. Logistic regression model results used to develop an urban probability surface for temperate, tropical, and arid regions based on biome designation.

		Coefficient	Standard error	t	p-value	AUC (%)
Temperate biomes[a]						**92**
	Intercept	6.30	0.08	74.31	0.00	
	$MaxEVI_{2009}$	-6.95	0.34	-20.44	0.00	
	$MaxEVI_{2010}$	-10.47	0.36	-29.35	0.00	
Tropical biomes[b]						**84**
	Intercept	-1.88	0.10	-18.71	0.00	
	$MaxEVI_{2009}$	5.72	0.41	13.81	0.00	
	$MaxEVI_{2010}$	5.83	0.44	13.23	0.00	
Arid biomes[c]						**76**
	Intercept	1.71	0.12	13.72	0.00	
	$MaxEVI_{2009}$	-3.50	1.09	-3.20	0.00	
	$MaxEVI_{2010}$	-3.99	1.10	-3.63	0.00	

a *Temperate biomes* include h26v04, h27v04, h27v05, h27v06, h27v07, h28v04, h28v05, h28v06, h28v07, h29v05, h29v06.

b *Tropical biomes* include tiles h28v07, h29v07, h30v07, h27v08, h28v08, h29v08, h30v08, h27v09, h28v09, h29v09, h30v09, h31v09, h32v09.

c *Arid biomes* include tiles h23v04, h24v04, h25v04, h23v05, h24v05, h25v05, h26v05, h25v06.

Table 5. Tier one accuracy (urban vs. non-urban land) by country, including user's and producer's accuracies for the urban class.

	Tier one accuracy (%)			Test sites (#)	
Country	Overall	Producer's	User's	Total	Urban
Myanmar	93	100	68	95	15
North Korea	93	88	64	67	8
South Korea	91	71	81	215	41
Laos	90	100	60	21	4
Cambodia	89	89	89	18	9
Thailand	87	73	58	324	51
Japan	86	91	74	563	185
Philippines	86	94	62	227	48
Indonesia	85	84	66	529	132
Singapore	85	89	80	20	9
Vietnam	85	77	68	209	53
China	83	85	62	4034	1042
Taiwan	80		0	5	0
Malaysia	79	97	60	201	63
REGION	**84**	**85**	**64**	**6528**	**1660**

Note: Cells left blank indicate there were no expansion sites drawn in the sample.

Table 6. Tier one accuracy (urban vs. non-urban land) by biome, including user's and producer's accuracies for the urban class.

	Tier one accuracy (%)			Test sites (#)	
Biome	Overall	Producer's	User's	Total	Urban
Temperate Conifer	100	100	100	16	2
Tropical Conifer	100	100	100	6	3
Mangrove	90	91	72	97	22
Temperate Grass	89	87	70	135	30
Flooded Grassland	89	92	69	53	12
Montane Grassland	87	92	57	76	13
Xeric Shrubland	86	83	74	81	24
Tropical Moist	85	89	61	2390	534
Tropical Dry	85	65	67	221	54
Temperate Mixed	83	84	65	3453	965
REGION	**84**	**85**	**64**	**6528**	**1659**

Table 7. The tier two sample design showing the number of sites in each strata (bold), and the share of urban land falling into each category (in parentheses).

a. Stratify by country

	Cambodia	China	Indonesia	Japan	Laos	Malaysia	Mongolia	Myanmar	N. Korea	Philippines	Singapore	S. Korea	Taiwan	Thailand	Vietnam
No. sites (%)	**20** (0.13)	**1324** (66.19)	**148** (7.32)	**243** (12.13)	**20** (0.08)	**67** (3.37)	**20** (0.2)	**20** (0.67)	**20** (0.3)	**36** (1.81)	**20** (0.29)	**40** (1.99)	**28** (1.42)	**39** (1.97)	**43** (2.13)

b. Stratify by biome

	Cambodia	China	Indonesia	Japan	Laos	Malaysia	Mongolia	Myanmar	N. Korea	Philippines	Singapore	S. Korea	Taiwan	Thailand	Vietnam
Tropical moist	**8** (0.4)	**267** (0.2)	**145** (0.99)	**2** (0.01)	**17** (0.83)	**67** (0.99)	-	**16** (0.82)	-	**36** (0.99)	**20** (1)	-	**28** (1)	**24** (0.62)	**24** (0.56)
Tropical dry	**12** (0.6)	-	**1** (0)	-	**3** (0.17)	-	-	**2** (0.08)	-	-	-	-	-	**6** (0.15)	**13** (0.3)
Tropical conifer	-	-	-	-	-	-	-	-	-	**0** (0.01)	-	-	-	-	-
Temperate mixed	-	**901** (0.68)	-	**231** (0.95)	-	-	-	-	**20** (1)	-	-	**40** (1)	-	-	-
Temperate conifer	-	**15** (0.01)	-	**10** (0.04)	-	-	-	-	-	-	-	-	-	-	-
Temperate grass	-	**62** (0.05)	-	-	-	-	**20** (1)	-	-	-	-	-	-	-	-
Flooded grass	-	**15** (0.01)	-	-	-	-	-	-	-	-	-	-	-	-	-
Montane grass	-	**45** (0.03)	-	-	-	-	-	-	-	-	-	-	-	-	-
Xeric shrub	-	**19** (0.01)	-	-	-	-	-	-	-	-	-	-	-	-	-
Mangrove	-	-	**1** (0.01)	-	-	**0** (0.01)	-	**2** (0.1)	-	-	-	-	-	**9** (0.23)	**6** (0.14)

Table 8. Tier two accuracy (urban vs. urban expansion) by country, including user's and producer's accuracies for the urban expansion class.

	Tier two accuracy (%)			Test sites (#)	
Country	Overall	Producer's	User's	Total	Expansion
Japan	91	100	17	243	5
North Korea	90	0		20	0
Taiwan	86	71	50	28	3
Mongolia	85	0		20	0
South Korea	82	71	59	40	10
Laos	80	75	86	20	7
Singapore	80	75	86	20	2
Indonesia	79	36	36	148	11
Malaysia	79	8	100	67	1
Philippines	78	100	33	36	5
Cambodia	75	71	71	20	7
Myanmar	75	33	50	20	2
Thailand	74	33	20	39	5
China	71	64	51	1324	166
Vietnam	70	53	80	43	15
REGION	**75**	**61**	**50**	**2086**	**419**

Note: Cells left blank indicate there were no expansion sites drawn in the sample.

Table 9. Tier two accuracy (urban vs. urban expansion) by biome, including user's and producer's accuracies for the urban expansion class.

	Tier two accuracy (%)			Test sites (#)	
Biome	Overall	Producer's	User's	Total	Expansion
Mangrove	89	72	91	18	2
Temperate Conifer	80	86	75	25	8
Temperate Grassland	78	43	33	82	9
Tropical Moist	76	46	45	654	99
Temperate Mixed	75	70	51	1192	273
Xeric Shrubland	74	40	67	19	3
Flooded Grassland	73	50	100	15	1
Montane Grassland	73	50	64	45	11
Tropical Dry	69	73	62	36	13
REGION	**75**	**61**	**50**	**2086**	**419**

Table 10. Confusion matrices for the tier one (a, b) and tier two assessments (c, d) before and after applying a 0.56 km^2 (3x3 pixel) minimum mapping unit (MMU).

Tier 1

a. All mapped built-up areas (n = 6528)

	Non-urban	Urban	k = 0.62
Non-urban	4075	794	84
Urban	243	1416	85
	94	64	**84%**

b. Minimum mapping unit applied (n = 6240)

	Non-urban	Urban	k = 0.64
Non-urban	3878	744	84
Urban	217	1401	87
	95	65	**85%**

Tier 2

c. All mapped built-up areas (n = 2086)

	Non-urban	Urban	Expansion	k = 0.36
Non-urban[a]	---	172	46	
Urban	---	1359	162	89
Expansion	---	133	211	61
		82	50	**75%**

d. Minimum mapping unit applied (n = 1956)

	Non-urban	Urban	Expansion	k = 0.39
Non-urban[a]	---	135	42	
Urban	---	1291	156	89
Expansion	---	123	207	63
		83	51	**77%**

a Note that the tier two validation assesses only two classes, urban land and urban expansion.

Table 11. The potential sources of error in the misclassified test sites of the tier two accuracy assessment.

	Issue	Occurrence (%)	Description, examples	Ground truth label 2000 » 2010[a]	Map label 2000 » 2010[a]	No. test sites
1	**Classification error**	35	Urban commission error where land without built surfaces is labeled urban land in 2010 (e.g. confusion between urban areas and extraction activities, riparian areas, bare soil, agriculture, etc.).	Non-urban » Non-urban	Urban » Urban	165
2	**Low density urban**	24	Area has some built-up areas c2000, but does not meet the >50% threshold to be considered urban. Because the area is labeled as urban c2000, it may result in either a change omission if the area increases to >50% built-up density by 2010 (a) or an urban commission if it remains >50% built-up (b).	Nonurban » Urban	Urban » Urban	71
				Nonurban » Nonurban	Urban » Urban	53
3	**Redevelopment and/or increasing built-up density**	20	New development occurs in existent urban area, e.g. settlement is cleared and rebuilt (a), or there is an increase in buildings/impervious cover (b), leading to change in spectral brightness. No change in label occurs.	Urban » Urban	Non-urban » Urban	105
4	**Change detection error**	19	Urban land and urban expansion are confused by classifier.	Urban » Urban	Non-urban » Urban	57
				Non-urban » Urban	Urban » Urban	41

a The labels in the table correspond to the class structure as follows: *Non-urban land* includes all non-urban -> non-urban areas; *Stable urban land* includes all urban -> urban areas; and *Urban expansion 2000-2010* includes non-urban -> urban areas.